A FRAGMENTATION APPROACH FOR CONCRETE IN COMPRESSION

Alberto CARPINTERI and Giuseppe FERRO
Politecnico di Torino, Dept. of Structural Engineering and Geotechnics, 10129 Torino, Italy.
email: carpinteri@polito.it, ferro@polito.it

Abstract

An experimental investigation on drilled cylindrical concrete specimens in compression over a large scale range (1:19) has been carried out to evaluate the variation of some mechanical parameters by varying specimen size. The peculiarity of the present investigation consists in exploring very small specimen dimensions. The experimental results show scale effects on dissipated energy density rather than on uniaxial compressive strength. A theoretical explanation for such a phenomenon, based on the fractal hypothesis, is presented and a comparison between experimental and theoretical values is discussed.

Introduction

Scale effects have received a strong interest in the last few decades. With the term *scale effects* both the variation of mechanical parameters as well as the variation of failure mode by varying the characteristic structural dimension (ductile to brittle transition) are considered. In tension, the phenomenon has been deeply discussed and important conclusions have been set. In particular, the variation of tensile strength was considered with the formulation of different laws. Bažant [1] defined the so-called Size Effect Law in the hypothesis of the presence of an initial crack of length proportional to the specimen size. This law has been often used in the literature. Successively, Carpinteri [2, 3] and Carpinteri et al. [4] proposed the Multifractal Scaling Law, valid for initially integer specimens and components. On the other hand, the compression failure is more complex and the related size effects are less understood.

The brittle failure in compression has been widely studied over the last decades. The phenomenon of axial splitting in the absence of confinement, as well as the related phenomena of exfoliation or sheet fracture, has been analyzed by Holzhausen and Johnson [5], by Nemat-Nasser and Horii [6] and by Ashby and Hallam [7]. Horii and Nemat-Nasser [8] have modeled the transition from brittle failure to ductile flow under very high confining pressures, by considering possible zone of plastically deformed materials at high shear-stress region around preexisting flaws. An interesting overview of brittle failure in compression can be found in [9].

The variation of the compressive strength with size and height-diameter (or slenderness) ratio is relevant when the rigid test machine platens are in direct contact with the concrete specimen, the lateral deformation of concrete being restrained at the specimen ends. In this context, a wide investigation has been carried out by Carpinteri et al. [10]. When, instead, the friction at the specimen ends is reduced, the strength variation is less evident [11].

An experimental investigation on geometrically similar cylindrical concrete specimens, obtained by a unique concrete block in compression over a very large scale range (1:19), will be brifly reported [12] and the obtained scale effects will be herein discussed. It will

be shown how, avoiding friction, the strength is almost independent of specimen dimension while strong variations are observed for dissipated energy density (DED). This phenomenon is interpreted by considering the fragmentation and the comminution theories. In this field, Fractal Geometry represents a very helpful tool to explain such a phenomenon.

Experimental investigation

The ambition of testing concrete specimen in compression in a very wide size range impacts strongly with the set-up, which opposes physical limits. The fundamental idea was to use a very simple standard testing apparatus composed only by a closed-loop servo-hydraulic system and strain gauges glued on the specimen to record the longitudinal as well as the transversal deformation in the pre-peak part of the force versus displacement curve.
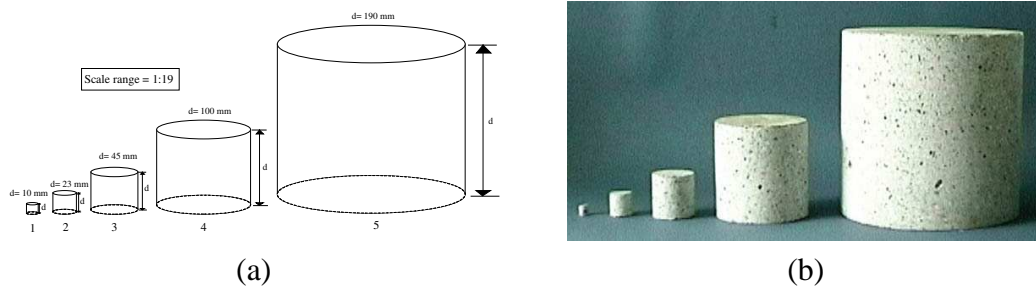

Figure 1: (a) Geometries of the five different concrete specimens; (b) overall view of the five specimen sizes.

All the cylinders were obtained by drilling from a unique concrete block with sizes 800 × 500 × 200 mm. The microconcrete used for the specimens is characterized by a maximum aggregate size of 4 mm . Five different diameters were considered in relation to the disposable drilling core-bits in a scale range of 1:19. The specimens were cylinders with a height/diameter ratio h/d =1 and d chosen as the characteristic dimension equal to 10, 23, 45, 100, 190 mm, respectively. Six specimens have been tested for d= 10 (C1), 23 (C2) and 45 (C3) mm and four specimens for d= 100 (C4) and 190 (C5) mm. The geometries of the tested specimens are presented in Fig. 1.a. The geometrical characteristics are reported in Ferro [12]. The nominal strength is 51.8 N/mm^2 while the compression strength of cube (150 × 150 × 150) after 28 days was equal to 33 N/mm^2. The water-cement ratio was equal to 0.65.

In uniaxial compression tests it is well-known how the boundary conditions play an important role. The system adopted in the present compression tests comes out from the analysis of the RILEM Technical Committee 148 SSC results [13] and consisted in using two teflon layers of 150 μm thickness with oil in between and a specimen slenderness equal to one.

The stress-deformation curves (Fig. 2.a) show an initial steadily increasing slope, due to the lower stiffness at the beginning of the test. After this initial part, the stress-strain path is nearly linear and this linear part is as more pronounced as larger the specimen is. The smaller the specimen, the more pronounced pre-peak nonlinearities are. After the peak stress, a gradual descending branch has been detected. The slope of the descending branch decreases with decreasing specimen height.

The values of the peak-stresses, which are commonly called *compressive strength*, are reported in Fig.2.b by varying specimen sizes. A marked size effect does not come out, as
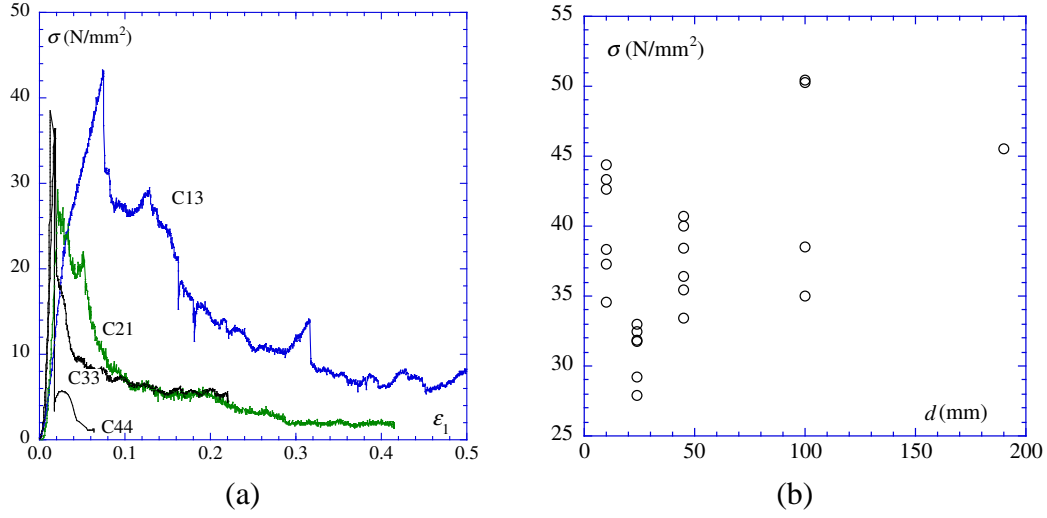
Figure 2: (a) Stress-strain curves for four different sizes; (b) peak-stresses by varying specimen size.

instead can be evidenced in tension [14] or in compression when localization is present [10]. The scatter in the results is not pronounced and even for the smallest size the values are comparable to the compressive strength of standard cubes. This permits to affirm that, if friction is avoided or drastically reduced, the compressive strength of an extisting concrete structure can be evaluated using very small drilling core specimens.

Fractal approach for the variation of DED with size

The performed compression tests have shown an evident decrease of dissipated energy density with increasing specimen dimension (Fig. 4). This interesting phenomenon can be interpreted by considering the fragmentation and the comminution theories. In this field, Fractal Geometry represents a very helpful tool. Fragmentation involves initiation and propagation of fractures. Fracture propagation is a highly nonlinear process requiring complex models even for the simplest configuration. Fragmentation involves the interaction between fractures over a wide range of scales. If fragments are produced over a wide range of sizes and if natural scales are not associated with the fragmented material, fractal distribution of number versus size would seem to be expected. The statistical number-size distribution for a large number of objects can be fractal [16].

Let us consider a concrete specimen which undergoes a compression test. In the postpeak softening regime the specimen is characterized by the generation of a large number of fragments. After fragmentation, the number of fragments N with a characteristic linear dimension greater than r should satisfy the relation:

$$N = \frac{B}{r^D},$$

(1)

where B is a constant of proportionality, and D is the fractal dimension.

In order to describe the mechanical meaning of the fractal exponent D, in Fig.3 some examples of discrete fragmentation model are presented, where fragmentation is a scale-invariant process that leads to a fractal distribution of chip sizes. We consider a fractal cube
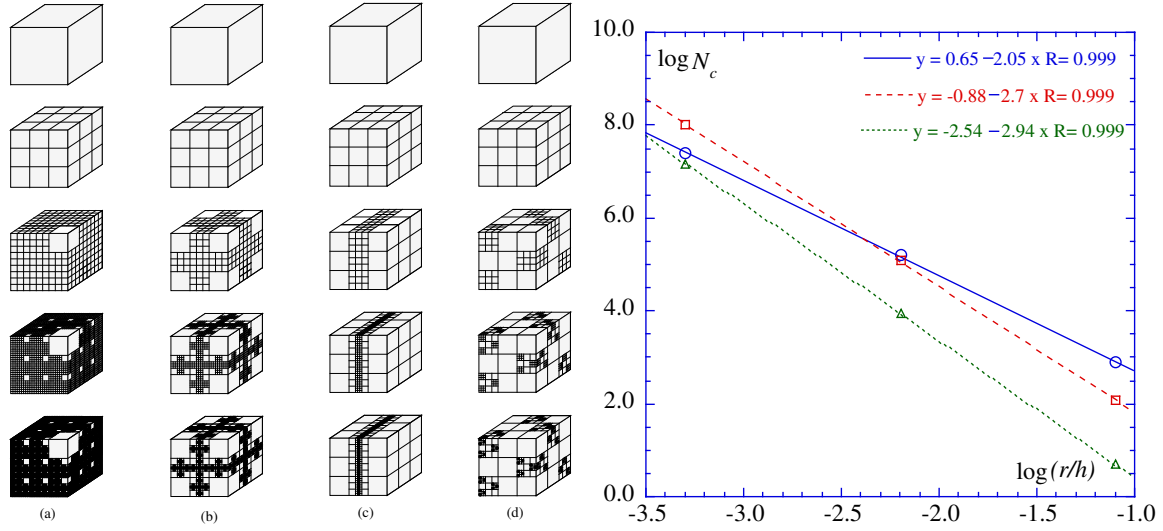
Figure 3: Physical meaning of exponent D; (a) at each step only one cube is retained, while all the others are divided into 27 equal-sized cubes with $r_n=\frac{1}{3}r_{n-1}$ (D=2.93), very close to a volumetric fragmentation; (b) at each step the eight angular cubes are retained, while all the others 19 are divided into 27 equal-sized cubes with $r_n=\frac{1}{3}r_{n-1}$ (D=2.70);(c) and (d) at each step the nine cubes are divided into 27 equal-sized cubes with $r_n=\frac{1}{3}r_{n-1}$, while the others 18 are retained (D=2.00), showing a localization of the dissipation energy; on the rigth cumulative statistics for the proposed fragmentation models.

and use it as the basis for a fragmentation model. The fragmentation is such that some blocks are retained at each scale but others are fragmented. In order to determine D, eq.(1) can be written as:

$$D = \frac{\log(N_{n+1}/N_n)}{\log(r_n/r_{n+1})},\qquad(2)$$

and then we can find for the three cases $D = \log 25/\log 3 = 2.93$ (Fig.3.a), $D = \log 19/\log 3 = 2.68$ (Fig.3.b) and $D = \log 9/\log 3 = 2.00$ (Fig.3.c,d), respectively. This is the fractal distribution of a discrete set. The cumulative number of blocks larger than a specified size for the three highest orders are $N_{1c} = 2$ for $r_1 = \frac{h}{3}$, $N_{2c} = 52$ for $r_2 = \frac{h}{9}$ and $N_{3c} = 1302$ for $r_3 = \frac{h}{27}$, obtaining a value $D = 2.95$ for the first example; $N_{1c} = 8$, $N_{2c} = 160$, $N_{3c} = 3048$ and $D = 2.70$ for the second example; $N_{1c} = 18$, $N_{2c} = 180$, $N_{3c} = 1638$ and $D = 2.05$ for the last two. The fractal dimensions for the discrete set and for the cumulative statistics are nearly equal.

Considering W as the global dissipated energy measured by the experimental set-up, $\mathcal{G}$ as the elastic energy release rate or the specific energy necessary to generate the unit area of fracture, which is by hypothesis invariant with respect to the scale of observation, we have:

$$W = \mathcal{G}A \quad \text{and then}: \quad \mathcal{G} = \frac{W}{A} = \frac{SV}{A} = \frac{Sl^3}{l^2} = Sl.\qquad(3)$$

If we consider a sequence of scale of observation, we have:

$$\mathcal{G} = S_1 l_1 = \ldots = S_{n-1} l_{n-1} = S_n l_n = S_{n+1} l_{n+1} = \ldots = S_\infty l_\infty,\qquad(4)$$

where the first scale of observation could be the macroscopic one, with $S_1 l_1 = Sl$, l being the characteristic linear dimension of the specimen, and the asymptotic scale of observation
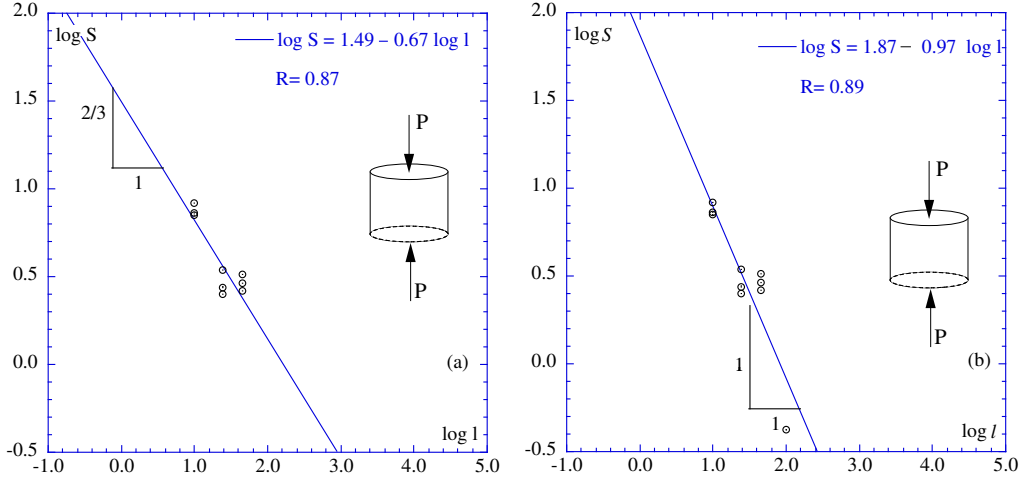
Figure 4: Size effect on dissipated energy density (experimental tests).

could be the microscopic one, with $S_\infty l_\infty = \mathcal{G}_F^* l^*$, l^* being the measure of the fractal set representing the fragmented configuration. From the equality between the extreme members we can write:

$$S = \mathcal{G}_F^* \left(\frac{l^*}{l} \right), \quad \text{or} \quad S = \mathcal{G}_F^* \left(\frac{l^{1-d_\omega}}{l} \right), \tag{5}$$

where $0 < d_\omega < 1$ is the decrement of the topological dimension due to nonhomogeneous fragmentation. Taking the logarithms of both members of eq.(5), we obtain:

$$\log S = \log \mathcal{G}_F^* - d_\omega \log l, \tag{6}$$

where $d_\omega = 3 - D$ can be considered as the decrement of the topological dimension of the set in which energy dissipation occurs. Eq.(6) represents a straight line with slope $(D - 3)$ in the $\log S$ versus $\log l$ plane (Fig.4). If $D = 2$, the slope is -1, as well as $D = 3$ implies a vanishing slope. For $D = 2$ (localization) $d_\omega = 1$; for $D = 3$ (volumetric dissipation) $d_\omega = 0$.

The two extreme cases are $D=2$, surface theory [15], when the dissipation really occurs on a surface ($W \propto V^{\frac{2}{3}}$), and by $D=3$, volume theory [16], when the dissipation occurs in a volume ($W \propto V$). In this case $\mathcal{G}_F^*$ presents the following physical dimensions:

$$[\mathcal{G}_F^*] = \frac{[F][L]^{-1}}{[L]^{D-2}} = [F][L]^{1-D}. \tag{7}$$

For $D = 2 \rightarrow [\mathcal{G}_F^*] = [F][L]^{-1}$, which is the canonical dimension for fracture energy, while for $D = 3 \rightarrow [\mathcal{G}_F^*] = [F][L]^{-2}$, which is the physical dimension of stress. The experimental cases of fragmentation are usually intermediate ($D \cong 2.5$) [17], as well as the size distribution for concrete aggregates due to Fuller [18].

The values of dissipated energy density for the three smallest sizes are plotted in Fig. 4.a against the specimen size in a bilogarithmic plane. The values for the four available sizes are instead reported in Fig.4.b. The size effect is represented by the slope of the linear regression

of the points of the diagram. It is evident how the dissipated energy density decreases with increasing specimen size.

As may be observed from Fig.4, the slope of the dissipated energy density decrease proves to be equal to 0.67 when only three specimen sizes are considered, and to 0.97 when considering the fourth size. We have considered the two different cases as the fourth size has been tested with a different procedure which can cause variations in energy estimation. The assumption of a fractal physical dimension allows the determination of the dissipated energy density parameter $\mathcal{G}_F^*$, which results to be independent of the scale. As it is easy to observe, in the latter case the renormalized dissipated energy density tends to be a fracture energy, the dissipation occurring on a fractal set very close to a 2-dimensional surface. Such a result confirms the localization of the dissipation on a surface [19]. The fractal nature of the fragments generated by the compressive test emerges very clearly at the size scale of the specimens. Momber [20] applied fragmentation theory to the study of compression and analyzed the fragments, determining a fractal exponent D close to 2. On the other hand, the property of self-similarity is very likely to vanish or change at higher or lower scales, owing to the limited character of the particle size curve.

Multifractal approach

The monofractal hypothesis provides a dissipated energy density $S = W/V \to 0$ for $l \to \infty$. Due to the limited validity of the self-similarity property, this is of course a physical nonsense. The same trend has been obtained in traction [3, 14], where the monofractal hypothesis was considered for cross-sectional ligaments. In that case, the geometrical multifractality of the cross-sectional material ligament [2, 4] permitted to determine the Multifractal Scaling Law for tensile strength, as well as for fracture energy [21] whenever the geometrical multifractality for fracture surface is assumed. The topological concept of geometrical multifractality, which can be also considered as an extension of the concept of self-affinity, may explain the inconsistencies shown in the preceding section. A self-affine fractal [22] is a fractal showing a different scaling law with respect to self-similarity, in the sense that a (statistically) similar morphology can be obtained only if the lengths are rescaled by direction-dependent factors. Such a fractal set can be identified by two different values of the fractal dimension: a local fractal dimension, in the limit of scales tending to zero, strictly equal to the Hausdorff topological dimension, and a global fractal dimension, corresponding to the largest scales, equal to the (integer) topological dimension.

On the other hand, it appears more consistent to deal with a continuous variation of the fractal dimension against the observation scale length (i.e. geometrical multifractality), than to consider only two limit values of the fractal dimension.

According to the previous considerations, the following multifractal scaling law for dissipated energy density (Fig.5) can be proposed [2, 4, 23]:

$$S = S_\infty \left(1 + \frac{l_{ch}}{l} \right), \tag{8}$$

where the two material constants S_∞ and l_{ch} can be obtained from fitting the experimental results. The physical requirements previously exposed are thus respected:
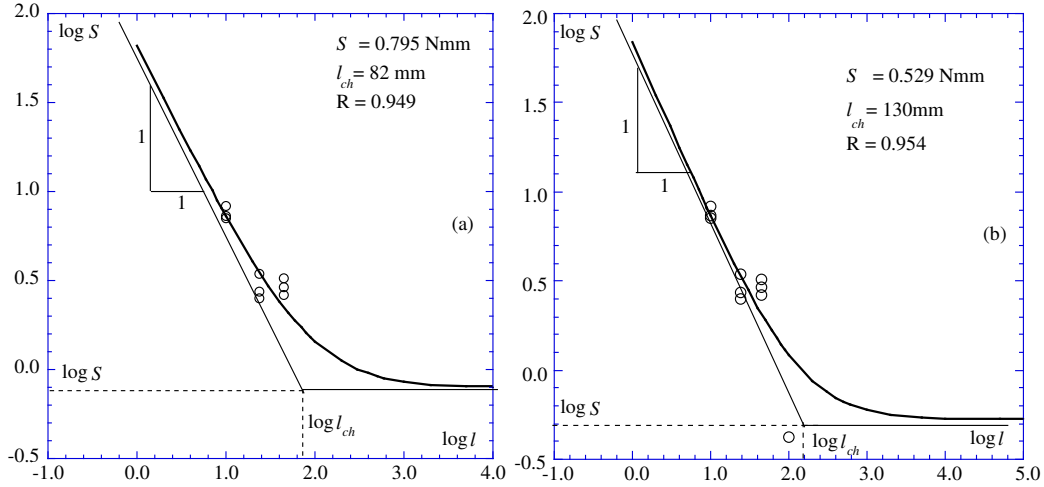
Figure 5: Bilogarithmic diagrams of dissipated energy density versus size: (a) three sizes; (b) four sizes.

$$\lim_{l \to +\infty} S_\infty \left(1 + \frac{l_{ch}}{l}\right) = S_\infty, \quad \lim_{l \to 0^+} S_\infty \left(1 + \frac{l_{ch}}{l}\right) = +\infty. \tag{9}$$

The horizontal coordinate of the intersection point of the two asymptotesis is equal to $\log l_{ch}$, with l_{ch} a characteristic length. This point ideally separates the disordered regime, where fragmentation is not homogeneous, from the ordered (homogeneous) regime. The microstructural characteristic size l_{ch}, in the case of normal-strength concrete, could be proportional to the maximum aggregate size d_{max}: $l_{ch} = \alpha \, d_{max}$.

It is reasonable to suppose that, for finer grained brittle materials (rocks, high-strength concrete) this value should be considerably smaller than in the case of normal-strength concrete, thus providing the curve to shift horizontally to the left in the bilogarithmic diagram.

The process, shows two asympthotes. At the smallest scales, the dissipation occurs over a domain very close to a surface ($D=2$), whereas at the largest scales the dissipation occurs over a domain close to a volume ($D=3$).

Conclusions

The uniaxial compression tests performed under displacement control on drilled cylindrical specimens obtained by a unique concrete block over a very large scale range (1:19) have confirmed as the scale effect on compressive strength is not as evident as in traction. The experimental results have instead manifested a strong scale effect on dissipated energy density, showing a sharp decrease of that quantity by increasing specimen size.

The hypothesis of energy dissipation in a sub-domain with physical dimension between 2 and 3 can be effective to justify such a phenomenon. It can be observed how, when energy dissipation occurs in the volume ($D=3$) no scale effects are present, whereas when energy dissipation occurs over an area ($D=2$) the scale effects are characterized in the bilogarithmic diagram $\log S$ versus $\log l$ by a linear law with slope equal to -1. By fitting the experimental values, we obtain an intermediate case, and a renormalized value for dissipated energy density, invariant with scale, can be obtained. This scale invariant value is characterized by

noninteger physical dimensions. This hypothesis works very well in the size range of the tested specimens.

In order to extend the trend of the dissipated energy density to all the size-scales, a multifractal law has been proposed, from which comes out how at small scales the failure is dominated by a fragmentation process (D=2) with severe scale effect, while at large scales the energy dissipation occurs in the volume (D=3) and the related scale effect vanishes.

Acknowledgements

References

1. Bažant, Z. P., *J. Engng. Mech. (ASCE)*, vol. **110**, 518–535, 1984.
2. Carpinteri, A., *Int. J. Sol. Struct.*, vol. **31**, 291–302, 1994.
3. Carpinteri, A., *Mech. Mater.*, vol. **18**, 89–101, 1994.
4. Carpinteri, A., Chiaia, B. and Ferro, G., *Mater. Struct.*, vol. **28**, 311–317, 1995.
5. Holzhausen, G. R. and Johnson, A., *Int. J. Rock Mech. Min. Sci. Geomech. Abstr.*, vol. **16**, 163–177, 1979.
6. Nemat-Nasser, S. and Horii, H., *J. Geoph. Res.*, vol. **87**, 6805–6821, 1982.
7. Ashby, M. F. and Hallam, D., *Acta Metal.*, vol. **34**, 497–510, 1986.
8. Horii, H. and Nemat-Nasser, S., *Phil. Trans. Roy. Soc. Lond.*, vol. **319**, 337–374, 1986.
9. Nemat-Nasser, S. and Hori, M., *Micromechanics, overall properties of heterogeneous materials*, North-Holland, Amsterdam, 1993.
10. Carpinteri, A., Ferro, G. and Monetto, I., *Mag. Concr. Res.*, vol. **51**, 217–225, 1999.
11. van Vliet, M. and van Mier, J., *Mech. Cohesive-Frict. Mater.*, vol. **1**, 115–127, 1996.
12. Ferro, G., *Private Comunication*, 2003.
13. RILEM TC 148-SSC, *Mater. Struct.*, vol. **30**, 195–209, 1997.
14. Carpinteri, A. and Ferro, G., *Materials and Structures*, vol. **27**, 563–571, 1994.
15. Rittinger, P. R., *Lehrbuch der aufbereitungskunde*, Berlin, 1937.
16. Kick, F., *Das gesetz der proportionalen widerstande*, Leipzig, 1885.
17. Turcotte, D. L., *Fractals and chaos in geology and geophysics*, Cambridge University Press, 1992.
18. Stroeven, P., in *Int. Symposium on Brittle matrix composites*, 1–10, Warsaw, Poland, 1991.
19. Lee, Y.-H. and Willam, K., *ACI Mater. J.*, vol. **94**, 457–471, 1997.
20. Momber, A., *Engng. Fract. Mech.*, vol. **67**, 445–459, 2000.
21. Carpinteri, A. and Chiaia, B., *Mater. Struct.*, vol. **28**, 435–443, 1995.
22. Mandelbrot, B. B., *Phys. Scripta*, vol. **32**, 257–260, 1985.
23. Carpinteri, A., Chiaia, B. and Ferro, G., *Mag. Concr. Res.*, vol. **49**, 45–53, 1997.